Društvo za tehniku
zavarivanja Slavonski Brod

12. Međunarodno znanstveno-stručno savjetovanje SBZ 2023

„STROJARSKE TEHNOLOGIJE U IZRADI ZAVARENIH KONSTRUKCIJA I PROIZVODA, SBZ 2023."
Slavonski Brod, 26. i 27. 04. 2023. i Požega 28. 04. 2023.

DISSIMILAR WELDING OF ALUMINUM ALLOYS 2024 T351 AND 6082 T6 BY TIG PROCESS

D. Milčić[1,*], M. Milčić[1], T. Vuherer[2], A. Đurić[3], D. Mitić[4], A. Radovanović[5]

[1]Faculty of Mechanical Engineering, University of Niš, Serbia
[2]University of Maribor, Faculty of Mechanical Engineering, Slovenia
[3]University of East Sarajevo, Faculty of Mechanical Engineering, Bosnia and Herzegovina
[4]NIVAR Niš, Čarnojevića 11/1, 18000 Niš, Serbia
[5]IMW Institut, Aleja Milanović bb, 34325 Lužnice, Kragujevac, Serbia

[*] Corresponding Author. E-mail: dragan.milcic@masfak.ni.ac.rs

Abstract

The aim of this work is to study the metallurgical and mechanical properties of dissimilar assemblies of 2024 T351 and 6082 T6 aluminum alloy by the TIG process. Aluminum alloy 6082 T6 is well weldable by classical fusion welding processes (MIG and TIG), while aluminum alloy 2024-T351 is almost non-weldable. Base metals were sheets with a thickness of 8 mm. The assembly of the plates was carried out by filler wire of an aluminum alloy type 4043A (AlSi5) with 2 mm of diameter. For the welding of these two Al alloys by TIG welding process in argon a shielding gas. The microstructural evolution across the welded joint dissimilar AA6082-T6 to AA2024-T351 aluminum alloy was characterized using optical and scanning electron microscopy (SEM). The hardness welded joint is the smallest in the melted area and the biggest on the side of 2024 alloy in HAZ. The fracture surface section of the tensile specimen is in the HAZ zone on the BM side - 6082-T6. The tensile strength of the welded joint is 166 MPa compared to 310 MPa for alloy 6082-T6 which is a weaker welded joint material, i.e. the reduction is about two times.

Keywords: 2024 and 6082 aluminum alloy, TIG welding, Microstructure, Mechanical properties

1. Introduction

Lightweight constructions are often used in transport technology in the automotive industry, in the rail vehicle industry, in shipbuilding, in the aviation industry and in space technologies. Different aluminum alloys are used for the production of light structures of transport vehicles due to the low density of the material, good mechanical properties, good corrosion resistance, etc. [1,2,3]. Often the structures of cars, trains, ships, planes and spacecraft are made by welding different aluminum

alloys. Welding of dissimilar aluminum alloys are made by MIG ([4, 5]) and TIG ([6]) TIG welding process, laser welding and electron beam welding ([7]) and friction stir welding (AA5754-AA7075 [8], AA2024-AA7075 [9], AA2219-AA5083 [10] and AA7075-AA6061 [11]). MIG and TIG fusion welding processes easily join aluminum alloys that have good weldability. A material is said to be well weldable if a certain welding procedure can produce such a welded joint with the least inhomogeneity in the welded joint. Particularly complex are cases of welding two different alloys (steel and stainless steel, different aluminum alloys 2024 and 6082, etc.) or welding fundamentally different types of materials (ceramics, metals, composites, etc.). TIG welding is widely used for welding different types of metals and metal alloys. TIG-welded aluminum alloys are used in various highly loaded constructions. Wide application of TIG welding is a consequence of small deformations, high quality and precise control of welding parameters [3]. If the technology of the TIG welding process is not suitable, defects may appear in the area of the welded joint, which reduces the reliability of the welded structure and thus the product. Possible defects when welding aluminum alloys are the lack of penetration, the formation of pores and inclusions, the formation of an Al_2O_3 oxidation layer on the surface of the metal due to the high affinity of aluminum to oxygen, and the appearance of hot cracks. [12]. Cracking occurs in aluminium alloys because of high stresses generated across the weld due to the high thermal expansion (twice that of steel) and the substantial contraction on solidification - typically 5 % more than in equivalent steel welds. In this paper, investigated the mechanical and structural property of butt joint dissimilar aluminum alloy AA2024 T351 and AA6082 T6 made by TIG welding process, was presented, where is it aluminum alloy 6082 T6 well weldable by classical fusion welding processes (MIG and TIG), while aluminum alloy 2024-T351 is almost non-weldable.

2. Experimental procedure and results

Chemical compositions and the mechanical properties of AA2024-T351 and AA6082-T6 are given in Tables 1.

Table 1. Chemical composition and mechanical propertie of the used metal AA2024 T351 and AA6082 T6

	Mn %	Fe %	Mg %	Si %	Cu %	Zn %	Ti %	Cr %	Al %
6082 T6	0,4…1,0	0 … 0,5	0,6 … 1,2	0,7 … 1,3	0 … 0,1	0 … 0,2	0 … 0,1	0 … 0,25	Balance
2024 T351	0,65	0,17	1,56	0,046	4,7	0,11	0,032		Balance

	Yield strength min R_{eh}/MPa	Ultimate tensile strength min R_m/MPa	Elongation at Break min A / %	Hardness HV
2024 T351	310	425	10	137
6082 T6	260	310	10	95

The Fronius Magic Wave 4000 Job G/F welding machine was used to weld the plates. The welding was performed under the protection of argon gas (Ar 5.0) with a purity greater than 99.999%. The dimensions of the plates used for welding were 300 mm long, 125 mm wide and 8 mm thick. The assembly of the plates was carried out by filler wire of an aluminum alloy type ALUMIG Si5 with 5% silicon (EN ISO 18273 S Al 4043A (AlSi5)). The chemical composition of the used filler material is given in Table 2.

Table 2. Chemical composition of the filler wire EN ISO 18273 S Al 4043A (AlSi5)

Mn %	Fe %	Mg %	Si %	Cu %	Zn %	Ti %	Be %	Al %
<0,15	<0,6	<0,2	4,5 … 5,5	<0,3	<0,1	<0,15	<0,0003	Balance

The welding parameters given in Table 3 were used for butt welding of plates.

Table 3. Welding parameters for the TIG welding process of butt welds for the material EN AW 2024-T351 / EN AW 6082-T6

Pass No.	Process number EN ISO 4063	Welding current *I* (A)	Welding voltage *U* (V)	Minimum preheat and inter pass temperature (°C)
1	141	225	13.3	40
2	141	235	13.1	90
3	141	195	13.3	90
4	141	195	13.3	90

Figure 1 shows the appearance of the face of a butt-welded joint. The welding was done with a backing strip. The macrostructure of the welded joint is shown in Figure 2.

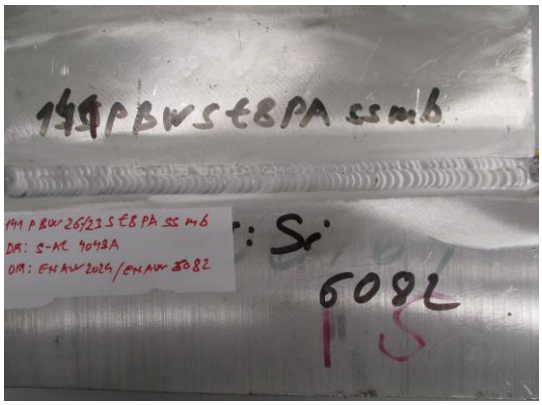

Figure 1. Appearance of the welded joint

Figure 2. Macro structure butt welded joints with backing strip butt welded joints with backing strip

Specimens were cut from the welded samples by water jet cutting. Test tubes were prepared for testing the macro- and microstructure of welded seams, for testing hardness, for testing impact

toughness using the Charpy impact test, tensile test specimen and bend test specimen. The microstructure of samples was examined by optical microscopy. Optical microscopy was performed by a Leica Q500MC microscope. Typical metallographic procedure implies using the Keller's and Barkerś reagent to expose morphology. Figure 3 shows the microstructures of the welded joint in the zones of the base materials, zones of heat influence and in the weld metal.

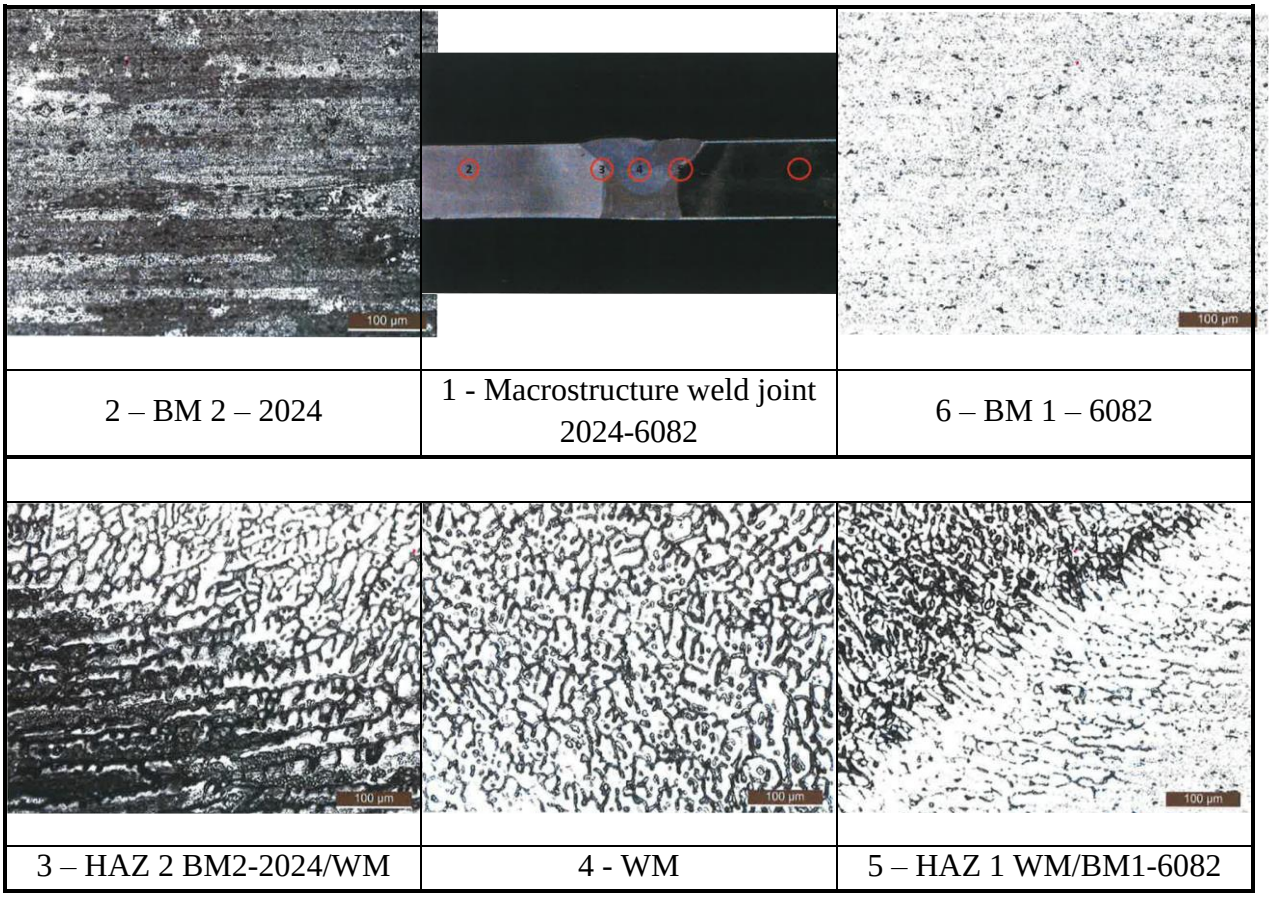

2 – BM 2 – 2024	1 - Macrostructure weld joint 2024-6082	6 – BM 1 – 6082
3 – HAZ 2 BM2-2024/WM	4 - WM	5 – HAZ 1 WM/BM1-6082

Figure 3. Microstructure of the welded joint

The hardness measurement was made in two lines, i.e., near the face and the root of the weld, three hardness measurements for each of the test zones (weld metal - WM, HAZ and base materials: BM1 – 6082 T6 and BM2-2024 T351), figure 4. The results of the hardness measurement of the welded joint are presented in Table 4

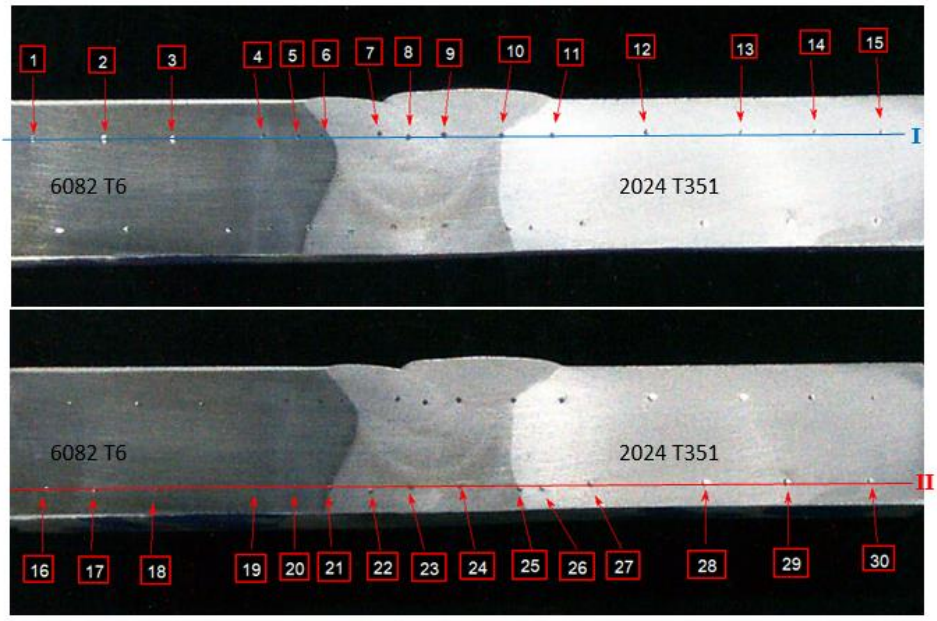

Figure 4. Places of hardness measurement on the welded joint

The results of the hardness measurements are given in Table 5, and the diagram of the hardness profile with measurements along two horizontal directions near the face and near the root of the welded joint is given in Figure 5.

Table 4. Hardness result for welded joint 2024 T351 – 6082 T6

Measurement place I / II	Hardness measurement weld zones	Hardness test results (HV)	Measurement place I / II	Hardness measurement weld zones	Hardness test results (HV)
1/16	BM 1	62.6/61.9	9/24	WM	60.9/57.4
2/17	BM 1	60.3/57.4	10/25	HAZ 2	110.1/88.6
3/18	BM 1	54.3/51.6	11/26	HAZ 2	98.4/87.3
4/19	HAZ 1	46.7/50.3	12/27	HAZ 2	96.7/89.3
5/20	HAZ 1	62.7/63.2	13/28	BM 2	92.1/110.5
6/21	HAZ 1	66.3/63.3	14/29	BM 2	111.4/117.2
7/22	WM	54.3/54.9	15/30	BM 2	117.4/123.0
8/23	WM	57.8/54.2			
BM 1– Base Metal 6082 T6 BM 2– Base Metal 2024 T351 HAZ 1 – heat affected zone BM 1 - WM WM – weld metal HAZ 2 – heat affected zone WM – BM 2					

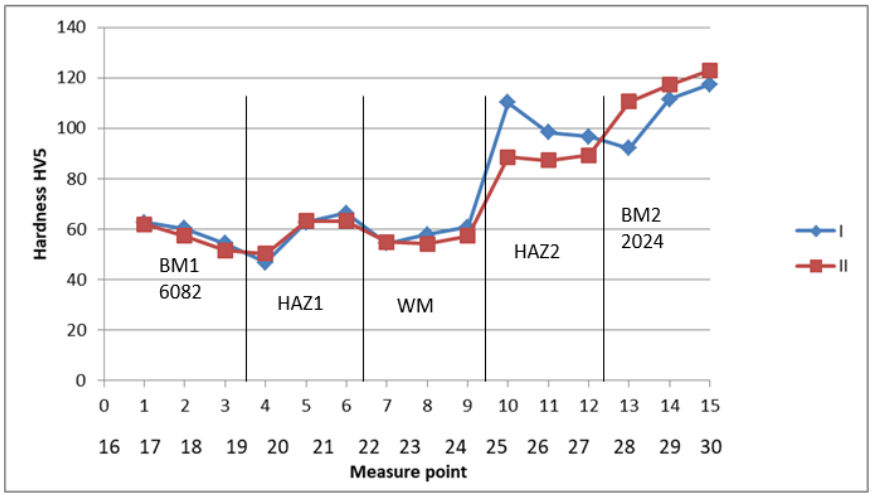

Figure 5. Hardness test results in BM 1, BM 2, HAZ 1, HAZ 2 and WM of butt weld joint with referring to the location in Figure 4

Tensile properties were estimated at room temperature using the Tensile Test System Shimadzu AG-X 300kN. Tensile specimens are made perpendicular to the welded joint. The dimensions of the tensile specimens are given in Figure 6. Figure 7 shows the tensile specimen after breaking.

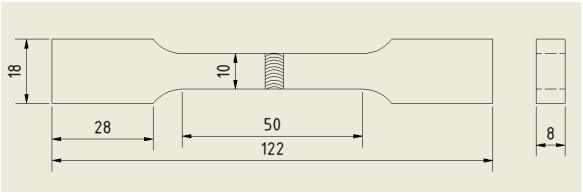

Figure 6. Dimensions of the tensile specimens

Figure 7. Tensile test fracture specimens

Stress-strain relationship of the tensile test is given in Figure 8, and the test results are shown in Table 5.

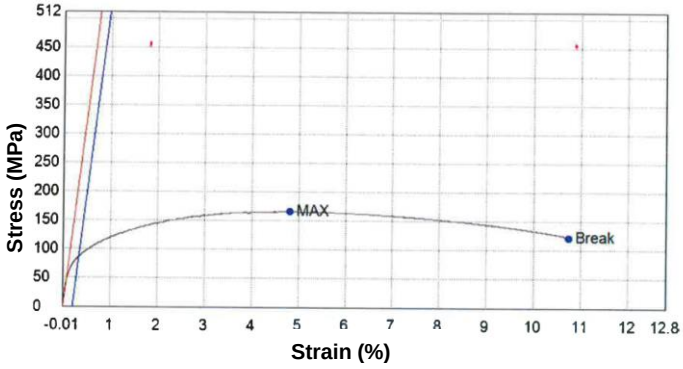

Figure 8. Relationship between stress and strain

Table 5. Tensil tests results

Cross□section area (mm^2)	Yield strength R_{eh} (MPa)	Ultimate tensile strength R_m (MPa)	Elongation after break A_{50} (%)	Fracture location
80	86	166	10.7	HAZ 1

Bend testing of the weld root and weld face of the welded joint dissimilar aluminum aloys are given in Figure 9 and 10. The test was performed at room temperature using the three-point bend test (Figure 8 and 9).

Figure 9. Bend testing of weld root

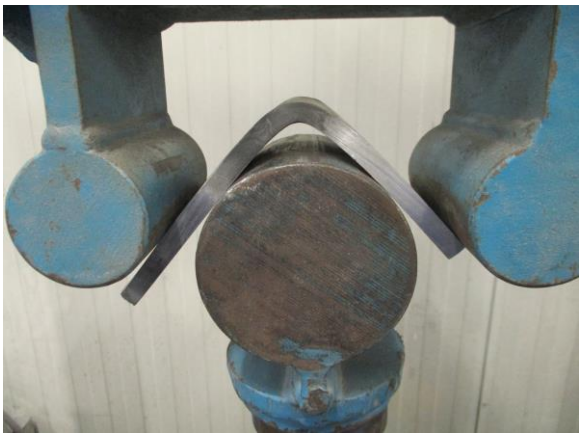

Figure 10. Bend testing of weld face

3. Discussion of results

Figure 3-1 presents the macrostructure of the welded joint observed on the cross-section of the weld axis. The joint has a regular symmetrical shape with visible underfilling of the weld face, without visible pores.

Figure 3-2 and 3-6 shows the microstructure of base materials: 2024 T351 aluminum alloy and 6082 T6 aluminum alloy. Elongated grains in the rolling direction were observed on the sample of 2024-T351 alloy. SEM/EDS analysis identified coarse intermetallic particles Al-Cu-Fe-Mn-Si (>10 μm), finer Al-Cu-Mg, Al-Cu-Mn, Al-Cu-Mg-Si and Al-Si-Cu-Mg (Figure 11). The fine particles can be precipitates of alloys elements, Al-Cu and Al-Cu-Mg based.

Microstructure of base metal – aluminum alloy 6082-T6, also consists of a wide range of intermetallic phases (IMP) formed during processing. Larger particles in the direction of rolling Al-Fe-Mn-Mg-Si-Cr, Al-Mg-Si-Mn, Al-Mg-Si (Figure 12), and fine precipitate particles Mg-Si, formed during the aging process were observed.

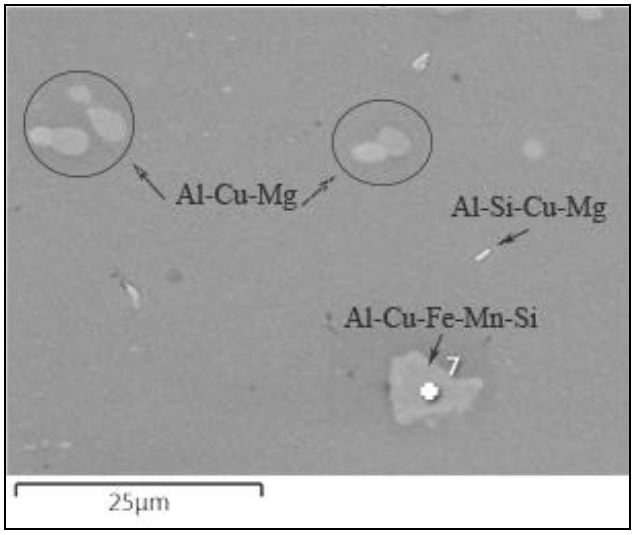

Figure 11. Second phase particles in 2024-T351 alloy. (SEM).

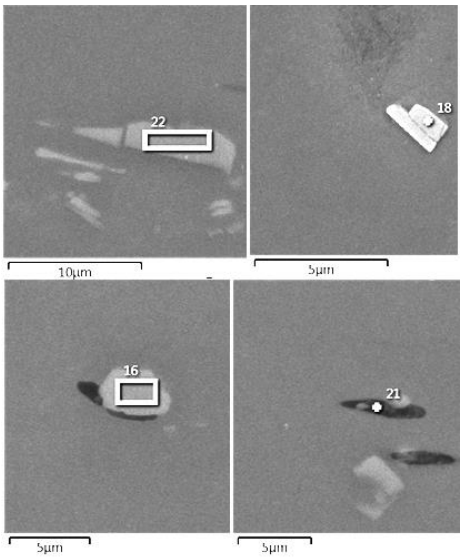

Figure 12. Second phase particles in 6082-T6 alloy. Al-Fe-Mn-Mg-Si-Cr, Al-Si-Mg, Al-Mg-Si-Mn, Al-Mg-Si. (SEM).

Figure 3-4 shows the microstructure of weld metal (WM) in TIG weld joints for dissimilar aluminum alloys (2024-T351 and 6082-T6). In WM are observed IMP precipitated on grain boundary and inside the grain. Depending of the place in WM coarse and fine grains can be found with dendritic orientation. Beside HAZ columnar orientation of the grain can be found.

Figure 3-5 shows the microstructure of the HAZ 1 between the weld metal and the base metal BM 1 - 6082 T6. In HAZ 1 are observed IMP precipitated on grain boundary with orientation in direction of rilling. Figure 3-3 shows the microstructure of the HAZ 2 between the weld metal and the base metal BM 2 - 2024 T351. In WM beside HAZ 2 are observed IMP precipitated on grain boundary with columnar orientation. In HAZ, are IMP precipitated on grain boundary and inside the grain. Grain orientation is in direction of rolling.

The section of the fracture surface of the tensile test specimen is shown in Figure 7. The location of the fracture is in the HAZ 1 area on the OM2 - 6082-T6 side. The yield strength is 3 times lower than the yield strength of the weaker base material in the 6082 T6 joint. The results of the bending test of the welded joint of two different aluminum alloys (2024 T351-6082 T6) indicate that deformation occurs in the weaker metal part of the aluminum alloy 6082 T6. The crack appears at a bending angle of approximately 90°. Looking at the hardness profile of the welded joint, the hardness of the weld metal is the lowest.

Fig. 5 shows the hardness test results of the butt weld joints. For AA6082 T6, the highest microhardness value was measured on the AA6082 T6 side, followed by the HAZ1 of AA6082 and the weld metal. For AA2024 T351, the lowest hardness value was on the HAZ2. Hardness decreased in the HAZ of both samples because of the effect of the heat treatment during the welding

process. The reduction in hardness could have resulted from recrystallization and/or grain growth because of the heat during welding [14].

5. Conclusions

The use of multi-materials structures is nowadays one of the most sought solutions to decrease weight and reduce both emission of greenhouse gases and fuel consumption in the automotive industry. In this paper, a study of the mechanical and metallographic properties of the welded joint of dissimilar aluminum alloys 2024 T351 and 6082 T6 made by the TIG welding process is given. Aluminum alloy 6082 T6 is well weldable by classic fusion welding processes, such as MIG and TIG processes. Unlike this aluminum alloy, alloy 2024 T351, which belongs to the group of aviation alloys, is considered almost non-weldable by classical welding procedures. For welding these two alloys, the technology is prescribed, and the filler bar EN ISO 18273 S Al 4043A (AlSi5) with 5% silicon is chosen.High silicon concentration leads to low melting temperature range, hence, giving high resistance to solidification cracking and undercut. The hardness is lower in the molten zone (WM) because the hardening precipitates are dissolved during melting and no structural hardening reaction takes place at this temperature. In the tensile test we have observed the fracture surface section of the tensile specimen is in the HAZ zone on the BM side - 6082-T6. The hardness of HAZ and WM at bottom surface of weldment of butt weld is higher than the upper surface.

Acknowledgments

This research was financially supported by the Ministry of Science, Technological Development and Innovation of the Republic of Serbia (Contract No. 451-03-47/2023-01/ 200109).

References

[1] Bohnart, Edvard R. TIG Handbook for GTAW Gas Tungsten Arc Welding. (2005). Miller Electric Manufacturing, LLC Company: Appleton, WI, USA.
[2] Muncaster, Peter W. A Practical Guide to TIG (GTA) Welding. (1991). Elsevier: Amsterdam, The Netherlands. (ISBN 10: 1855730200, ISBN 13: 9781855730205)
[3] Larry, Jeffus. Welding: Principles and Applications; DELMAR Cengage Learning: Boston, MA, USA, 2016. (ISBN-13: 978-1-1110-3917-2)
[4] Lean, P.P; Gil, L; Ureña, A. Dissimilar welds between unreinforced AA6082 and AA6092/SiC/25p composite by pulsed-MIG arc welding using unreinforced filler alloys (Al–5Mg and Al–5Si). (2003). Journal of Materials Processing Technology, Volumes 143–144, 846-850. https://doi.org/10.1016/S0924-0136(03)00331-5
[5] Nawres Jabar Nasser, Mechanical Properties of MIG Joints for Dissimilar Aluminum Alloys (2024-T351 and 6061-T651). (2016). Al-Khwarizmi Engineering Journal, 12(3), 121- 128

[6] Liamine Kaba, Mohammed Elamine Djeghlal, Seddik Ouallam, Sami Kahla, Dissimilar welding of aluminum alloys 2024 T3 and 7075 T6 by TIG process with double tungsten electrodes. (2022). The International Journal of Advanced Manufacturing Technology, 118, 937–948. https://doi.org/10.21203/rs.3.rs-408163/v1

[7] Himanshu Lalvani, Paranjayee Mandal, Cold forming of Al-5251 and Al-6082 tailored welded blanks manufactured by laser and electron beam welding. (2021). Journal of Manufacturing Processes, 68, Part A, 1615-1636. https://doi.org/10.1016/j.jmapro.2021.06.070

[8] Kasman, Şefika, Yenier, Zafer. (2014). Analyzing dissimilar friction stir welding of AA5754/AA7075. The International Journal of Advanced Manufacturing Technology, 70(1-4), 145-156. https://doi.org/10.1007/s00170-013-5256-7

[9] Youbao, Song; Xinqi, Yang; Lei, Cui; Xiaopeng, Hou; Shen, Zhikang; Xu, Yan. (2014). Defect features and mechanical properties of friction stir lap welded dissimilar AA2024–AA7075 aluminum alloy sheets. Materials & Design, 55, 9-18. https://doi.org/10.1016/j.matdes.2013.09.062

[10] Mastanaiah, P.; Sharma, Abhay; Reddy, Madhusudhan, G. (2016). Dissimilar friction stir welds in AA2219-AA5083 aluminium alloys: effect of process parameters on material inter-mixing, defect formation, and mechanical properties. Transactions of the Indian Institute of Metals, 69(7), 1397-1415. https://doi.org/10.1007/s12666-015-0694-6

[11] Hasan, Mohammed M.; Ishak, Mahadzir; Rejab, Ruzaimi. (2017). Influence of machine variables and tool profile on the tensile strength of dissimilar AA7075-AA6061 friction stir welds. The International Journal of Advanced Manufacturing Technology, 90(9-12), 2605-2615. https://doi.org/10.1007/s00170-016-9583-3

[12] https://www.twi-global.com/technical-knowledge/job-knowledge/weldability-of-materials-aluminium-alloys-021 (access 04.03.2023)

[13] https://www.matweb.com (access 04.03.2023)

[14] Durmuş, H.; Çömez, N. (2017). Mechanical Properties of AA5754 Sheets Welded by Cold Metal Transfer Method, Technological Applied Sciences (NWSATAS), 12(4), 170-177. doi:10.12739/NWSA.2017.12.4.2A0124.